Korean J. Chem. Eng., 33(9), 2538-2546 (2016)
DOI: 10.1007/s11814-016-0095-5

pISSN: 0256-1115
eISSN: 1975-7220

A two-dimensional discrete lumped model for a trickle-bed vacuum gas oil hydrocracking reactor

Sepehr Sadighi†

Catalysis Research Division, Research Institute of Petroleum Industry (RIPI), P. O. Box 14665137, Tehran, Iran
(*Received 19 January 2016 • accepted 2 April 2016*)

Abstract−A two-dimensional (2D) computational fluid dynamics model based on discrete lumping approach was used to predict the product yields of a pilot scale vacuum gas oil (VGO) hydrocracking reactor. This model was developed by solving mass conservation equations in conjunction with the continuity and momentum balances in the z-r cylindrical plane. The kinetic parameters of the model were estimated from the experimental data, and validated by using actual values. Results show that the proposed model can appreciably improve the accuracy of the yield prediction in comparison to the predicted value using the 1D model. Moreover, it is confirmed that the order of magnitude of the radial liquid velocity against the axial one is considerably low, and there is no significant pressure drop along the r-direction. Additionally, results show that two-dimensional model is a reliable tool for evaluating the catalyst performance and also for designing commercial reactors.

Keywords: Hydrocracking, Computational Fluid Dynamics, Trickle Bed Reactor, Discrete-lump Model

INTRODUCTION

Hydrocracking is an important secondary process in the petroleum industry that is generally used to process feed stocks ranging from vacuum gas oil (VGO) to residue [1-3]. With the attention to the profit margin, hydrocracking is widely interesting due to its flexibility for upgrading heavy feedstock into light precious products, such as naphtha, kerosene and diesel. Moreover, it is an interesting process in a refinery that upgrades the quality and the quantity of refined petroleum products simultaneously [4].

Similar to other refining and petrochemical processes, optimal operation is required to guarantee profitability and productivity. Therefore, a kinetic model can be beneficial to finding optimum operating conditions [5-7]. Ideally, the kinetic model should take into account all the elementary reactions. However, describing hydrocracking reactions at a molecular level is very difficult due to the complexity of mixture and variety of components. To simplify the problem, a lumping approach has been adopted to study the effect of operating parameters on the distribution and composition of the hydrocracking products [8].

The major lumping methods of interest in this field are continuum theory of lumping and discrete lumping approaches. In the first method, the reactive mixture is assumed to form a continuum mixture with respect to its properties such as boiling point, molecular weight, carbon number or chemical species [9,10]. But, in the discrete lumping approach, the reaction network is reduced to a limited number of reactions. Lumps based on compound types (e.g., diesel, kerosene, gasoline, etc.) are often defined based on their boiling points.

According to the discrete lumping approach, there are many researches in which the hydrocracking process is modeled with three-lump [11,12], four-lump [13,14], five-lump [15], six-lump [16] and eight-lump [17] partitions. In all these studies, the pilot or industrial scale reactor was modeled using a one-dimensional (1D) space in which hydrocracking and/or hydrotreating reactions were assumed to be carried out in the axial direction. According to the literature [18], even for a fixed-bed system used for the methanol and synthesis gas production, the profile of the mole fraction is not sensitive to the radial variation in the bed structure, but the viscous forces can be significant. Therefore, the consideration of viscous, gravitational, drag and pressure forces can also improve the predictability of VGO hydrocracking model. Recent advances in computational fluid dynamics (CFD) show promising results in understanding fluid dynamics and its interactions with chemical reactions. Thus, many studies have been recently performed for CFD modeling of trickle bed reactors (TBRs) [19-23].

The current study is devoted to developing an applicable 2D CFD model for a VGO hydrocracking reactor in the trickle-bed regime by using the lumping approach. This model is capable of predicting yield of hydrocracking products, i.e., gas, naphtha, distillate and residue. To perform such a task, a four-lump kinetic network is applied and governing transport equations (continuity, species conservation and momentum) are solved simultaneously through the catalytic bed in the z-r cylindrical plane. Then, the required kinetic parameters of the model are estimated from the experimental data. After estimating parameters of the model and simulating the yield of product, discussions are presented to compare results of 2D model against those of 1D one. Moreover, other significant variables such as radial velocity, pressure drop and liquid hold up are studied using the proposed model.

†To whom correspondence should be addressed.
E-mail: Sadighis@ripi.ir, sadighi_sepehr@yahoo.com

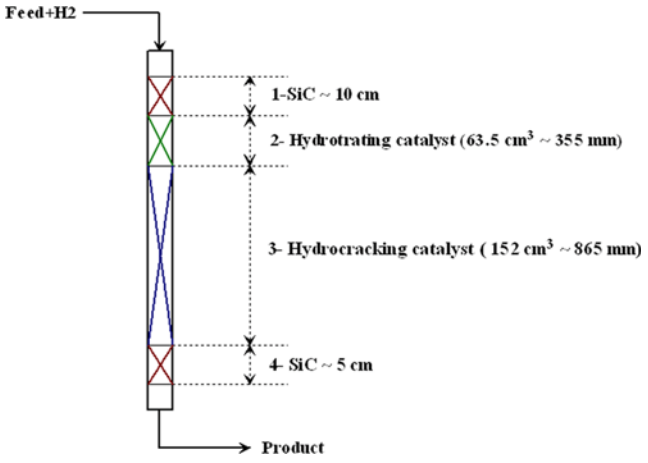

Fig. 1. Sections of catalytic reactor bed.

EXPERIMENTAL DATA

In this research, the same data for developing a 1D combined-bed kinetic model is used [24]. The device, catalyst, feed and operating conditions were described completely in the previous work [25]. The reactor consisted of a cylindrical vessel with an internal diameter of 0.016 m and height of 1.22 m (see Fig. 1). The entrance of the catalytic bed was packed with 0.1 m of inert SiC particles to provide a uniform distribution of gas and liquid. The catalytic bed was loaded with 6.35×10^{-5} m^3 of hydrotreating and 1.52×10^{-4} m^3 of hydrocracking catalysts, respectively. Additionally, the outlet of the catalytic bed was also loaded with SiC to provide a well-mixed stream at the outlet of the reactor.

Fresh VGO, recycle stream and distillate samples were analyzed according to the ASTM D1160 standard procedure while naphtha samples was analyzed according to the ASTM D86 method. Moreover, an Anton Paar viscometer (model SVM 3000) was used for measuring viscosity of feed and products according to ASTM 445 test procedure. All required densities were measured using ASTM 5002 standard method.

In this research, commercial hydrotreating (HDT) and hydrocracking (HDC) catalysts were used. Specifications of these catalysts are presented in Table 1. Before charging the feed, both catalysts were heated to 130 °C and held at this temperature for 6 h. Then, they were sulfided with an appropriate agent according to the procedure of the catalyst supplier.

The feed was prepared by blending of fresh VGO and recycle feed (unconverted oil) which were taken from a commercial scale plant. Feed properties are shown in Table 2. Mixing ratio of fresh and recycle feeds was 83.3 vol% and 16.7 vol%, respectively. The pilot scale experiments were carried out under the following process conditions: (1) H_2/HC of 1,357 Nm^3/Sm^3; (2) LHSV of 0.8, 0.9 and 1.05 h^{-1}; (3) Temperature of 360 °C, 370 °C, 380 °C and 390 °C, and (4) Pressure of 146 bar. The range of these variables was selected according to the recommendation of the catalyst manufacturer.

Table 2. Properties of fresh VGO and recycle feed

Property	Fresh VGO	Recycle feed
SP.GR@15.56 °C	0.8777	0.8738
Distillation range (vol%)		
ASTM D1160	°C	°C
IBP	329.7	287.8
10%	390.6	390.7
30%	423.2	430.1
50%	445.6	452.9
70%	475.1	478.3
90%	523.7	517.1
End point	567.1	561.3
Nitrogen (ppmwt)	800	200
Sulfur (wt%)	1.4	0.03
Aromatics (wt%)	34	14.5
Asphalt & resin (wt%)	<0.1	<0.1

Table 3. Average properties of hydrocracking product

Lump	IBP-FBP (°C)	Sp.g @15 °C	Mw	Molar vol. (cm^3/gmol)	Viscosity* (Pa·s)
Gas	40^-	0.35	38	-	$9.258*10^{-6}$
Naphtha	40-160	0.75	113.8	0.1515	$1.957*10^{-4}$
Distillate	161-370	0.823	220.3	0.2647	$1.626*10^{-3}$
VGO	370^+	0.89	420	-	$6.105*10^{-2}$

MODEL FORMULATION

We used a four-lump mathematical model, including VGO, distillate, naphtha and gas partitions, to simulate the main products of the pilot scale plant (Table 3). Fig. 2 illustrates the process pathways associated with the mentioned strategy. In this approach,

Table 1. Characteristics of HDT&HDC catalysts

Property	HDT	HDC
Size & shape	1/16″ & Quadralobe	1/16″ & Cylindrical
Color	Green	Brown
Bulk density (kg/m^3)	750	850
BET surface area (m^2/g)	186.56	199.46
Langmuir surface area (m^2/g)	259.20	273.71
Average pore diam (A^0)	89.09	69.14
Main ingredients	Mo, Ni, Ti	Zr, W, Ni, Si, Al

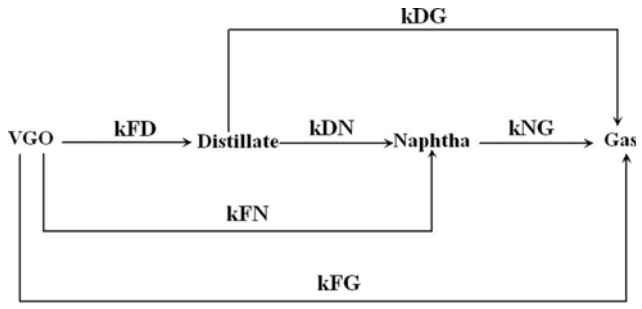

Fig. 2. The complete four-lump kinetic model.

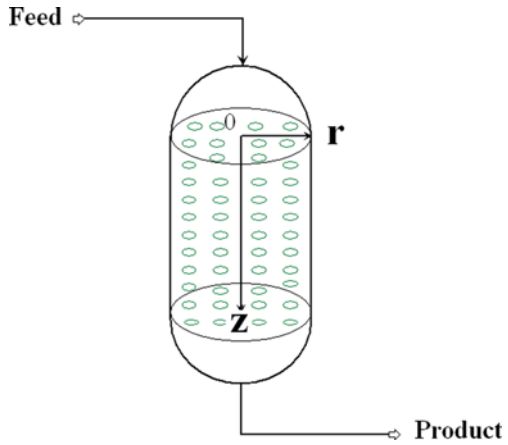

Fig. 3. Model geometry for the 2D hydrocracking reactor.

called combined bed model, hydrogen consumption is neglected. It is obvious that during hydrocracking and hydrotreating reactions, hydrogen molecules are absorbed in the hydrocarbon structure, but sulfur and nitrogen are removed. As shown in the previous work, this assumption can only impose 1% error in the mass balance which is ignorable [24].

To model this reactor, which works in the trickle-bed regime, it is assumed that the variations around the central axis are negligible. Hence, a two-dimensional symmetric geometry can be applied (see Fig. 3). Throughout the catalytic bed, both liquid and gas (mostly hydrogen and sour gases) flow downward co-currently, and hydrocracking reactions are carried out. Because the volume flow rate of liquid in comparison with gas at high pressure is lower, the liquid cannot saturate the void fraction of bed, and there is a two-phase regime through the catalytic bed. To simplify two-phase model, it is assumed that (1) the VGO feed and the products are all in the liquid phase, and (2) due to the large amount of excess hydrogen and also high pressure, the gas phase mostly belongs to pure hydrogen. Therefore, the variation of hydrogen mass flow rate in the axial and radial directions is negligible.

Like a porous media in which the void space is occupied by gas and liquid phases, the void fraction of bed (ε) is filled with liquid and hydrogen. Accordingly, the fraction of liquid in the void of catalytic bed (S_l) is calculated as follows:

$$S_l = \frac{\dot{v}_m + \dot{v}_{H_2}}{\dot{v}_m} \tag{1}$$

here, $\dot{v}_m$ and $\dot{v}_{H_2}$ are the volume flow rate of the liquid stream and hydrogen, respectively.

Additionally, the following assumptions are made to solve the governing equations:

1- Hydrocracking is a first-order hydrocracking reaction and since hydrogen is present in excess, the rate of hydrocracking is independent of hydrogen concentration.

2- The pilot reactor operates under isothermal conditions.

3- Hydrogen feed is pure.

4- There is uniform void distribution through the bed.

5- The intra-phase exchanges between gas and liquid are negligible.

6- Unit operates in steady state condition.

7- Coke deposition, poisoning by sulfur and metals, sintering and loss of active surface are not included in the model [26]. Therefore, simulation is only valid for the start of run conditions.

8- The molecular diffusion of naphtha and distillate in the product stream obeys Fick's law. Moreover, distillate and naphtha are dilute solutes in the VGO stream.

For examining the importance of axial mixing, a widely accepted empirical criterion is applied as follows [27]:

$$\frac{L}{d_p} \geq 100 \text{ and } \frac{D_r}{d_p} \geq 10 \tag{2}$$

where L is the length of the bed; d_p is the diameter of the catalyst particle, and D_r is the internal diameter of the reactor. According to the presented data for the understudy reactor, the above criteria are relatively satisfied. Therefore, ignoring the axial dispersion cannot impose considerable error into the model.

For each reaction, the kinetic expression is formulated as the function of mass concentration and kinetic parameters (k_0, E). Based on the mentioned assumptions, rate constants of the proposed model are as follows:

Vacuum gas oil or Feed (F): $$k_{Fj} = k_{0Fj} \exp\left(\frac{-E_{Fj}}{RT}\right) \tag{3}$$

Note that j in Eq. (3) represents distillate (D), naphtha (N) and gas (G)

Distillate (D): $$k_{Dj'} = k_{0Dj'} \exp\left(\frac{-E_{Dj'}}{RT}\right) \tag{4}$$

j′ in Eq. (4) represents naphtha (N) and gas (G).

Naphtha (N): $$k_{NG} = k_{0NG} \exp\left(\frac{-E_{NG}}{RT}\right) \tag{5}$$

In Eqs. (3) to (5), T and R are the bed temperature and ideal gas constant, respectively.

Consequently, the reaction rates (R_j) can be formulated as the following:

Vacuum gas oil reaction (R_F): $$R_F = \sum_{j=D}^{G} k_{Fj} C_F \tag{6}$$

Finally, the reaction rates for hydrocracking products can be described as follows:

Distillate (R_D): $$R_D = k_{FD} C_F - \sum_{j'=N}^{G} k_{Dj'} C_D \tag{7}$$

Naphtha (R_N): $$R_N = k_{FN}C_F + k_{DN}C_D - k_{NG}C_{NG} \quad (8)$$

Gas (R_G): $$R_G = \sum_{j=F}^{N} k_{jG}C_j \quad (9)$$

To model the reactor, the partial differential equations (PDE) of continuity and Navier-Stokes equations should be solved for the flow in a porous media, which are written as follows [28]:

$$\frac{1}{\varepsilon_l}\frac{\partial}{\partial z}(\rho u) + \frac{1}{\varepsilon_l}\frac{1}{r}\frac{\partial}{\partial r}(r\rho v) = 0 \quad (10)$$

$$\frac{\rho u}{\varepsilon_l}\frac{\partial u}{\partial z} + \frac{\rho v}{\varepsilon_l}\frac{\partial u}{\partial r} = \frac{\mu}{\varepsilon_l}\frac{\partial^2 u}{\partial z^2} + \frac{\mu}{\varepsilon_l r}\frac{\partial}{\partial r}\left(r\frac{\partial u}{\partial r}\right) - \frac{\partial P}{\partial z} + \rho g_z - F_u \quad (11)$$

$$\frac{\rho u}{\varepsilon_l}\frac{\partial v}{\partial z} + \frac{\rho v}{\varepsilon_l}\frac{\partial v}{\partial r} = \frac{\mu}{\varepsilon_l}\frac{\partial^2 v}{\partial z^2} + \frac{\mu}{\varepsilon_l}\frac{\partial}{\partial}\left(\frac{1}{r}\frac{\partial}{\partial r}(rv)\right) - \frac{\partial P}{\partial r} + \rho g_r - F_v \quad (12)$$

$$\varepsilon_l = \varepsilon \cdot S_l \quad (13)$$

where u and v are superficial liquid velocities in the axial (z) and radial (r) directions through the catalytic bed, respectively; ε is the volume void fraction of the catalytic bed (0.65); ε_l is the liquid hold up of the catalytic bed; P is the pressure of the reactor, and g_z (9.086 m/s^2) and g_r are the gravitational forces. The latter is equal to zero for the system studied. Moreover, the friction factor (F) is calculated by using the Ergun correlation as follows:

$$F = \left[\frac{150\mu}{d_p^2}\left(\frac{(1-\varepsilon_l)^2}{\varepsilon_l^3}\right)U + \frac{1.75\rho}{d_p}\left(\frac{(1-\varepsilon_l)}{\varepsilon_l^3}\right)U^2\right] \quad (14)$$

where U represents u and v for calculating F_u and F_v.

Furthermore, the species conservation in the trickle bed regime should be solved simultaneously in conjunction with the continuity and Navier-stokes equations. Because of low Reynolds number of the stream ($9<Re_p<25$), molecular diffusion is important. Therefore, the mass transport equation for lumps can be expressed as follows:

$$\frac{\partial}{\partial z}(C_j u) + \frac{1}{r}\frac{\partial}{\partial r}(C_j r v) \pm \eta(1-\varepsilon)R_j = D_{jF}\frac{\partial^2 C_j}{\partial z^2} + \frac{D_{jF}}{r}\frac{\partial}{\partial r}\left(\frac{\partial(rC_j)}{\partial r}\right) \quad (15)$$

where j ranges from the fresh feed (F) to gas (G); C denotes the mass concentration of lumps; η is the effectiveness factor which is equal to 0.7 for a cylindrical catalyst in a trickle bed regime [29]; the positive sign "+" stands for reactant (feed or VGO); the negative sign "−" relates to products, and D_j is the dispersion of lumps in the VGO feed whilst the self-diffusion and diffusion of gas in VGO are neglected. Therefore, D_{FF} and D_{GF} are equal to zero.

Due to the low Reynold number and axial dispersion through a TBR [30], the dispersion of naphtha and distillate to VGO is calculated by using Wilke-Chang equation as follows:

$$D_{jF} = 7.4\times10^{-8}\times\frac{\sqrt{Mw_F}T}{\mu V_j^{0.6}} \quad (16)$$

where Mw and V (cm^3/gmole) are the molecular weight and molar volume of lumps, respectively (see Table 3). Additionally, the viscosity of bulk stream (μ) should be expressed as centipoise (cp) to yield the molecular diffusivity in cm^2/s.

In Eqs. (9) to (15), ρ and μ are the density and viscosity of stream at hydrocracking pressure and temperature, respectively. These transport parameters can be calculated as follows [31]:

$$\frac{1}{\rho} = \sum_{j=F}^{G}\frac{Y_j}{\rho_j} \quad (17)$$

$$\ln\mu^{\frac{1}{3}} = \sum_{j=F}^{G} Y_j \ln\mu_j^{\frac{1}{3}} \quad (18)$$

$$Y_j = \frac{C_j}{\sum_{j=F}^{G} C_j} \quad (19)$$

where ρ_j and μ_j are the density and viscosity of lumps at the pressure and temperature of the reactor. The values of transport properties for the hydrocracking lumps at corresponding temperatures and also the reactor pressure are presented in Table 4. Because the pressure drop through the catalytic bed is less than 100 kPa (will be discussed later), properties are calculated at the average pressure.

Now, the described PDEs should be solved subjected to the boundary conditions. Fig. 4 illustrates the boundary conditions (B1-B4) as follows:

Table 4. Properties of hydrocracking lumps at the reactor condition

Density @146 bar (kg/m^3)				
Lump	T=360 °C	T=370 °C	T=360 °C	T=370 °C
Gas	110.27	107.89	105.62	103.62
Naphtha	466.08	453.68	441.33	429.08
Distillate	628.32	621.88	615.59	608.47
VGO	658.29	652.05	645.95	639.65
H_2	5.398	5.316	5.237	5.160
Viscosity @146 bar (Pa·s)				
Lump	T=360 °C	T=370 °C	T=360 °C	T=370 °C
Gas	$2.413*10^{-5}$	$2.426*10^{-5}$	$2.438*10^{-5}$	$2.446*10^{-5}$
Naphtha	$8.757*10^{-5}$	$8.456*10^{-5}$	$8.159*10^{-5}$	$7.868*10^{-5}$
Distillate	$1.193*10^{-4}$	$1.147*10^{-4}$	$1.103*10^{-4}$	$1.062*10^{-4}$
VGO	$3.777*10^{-4}$	$3.572*10^{-4}$	$3.383*10^{-4}$	$3.206*10^{-4}$

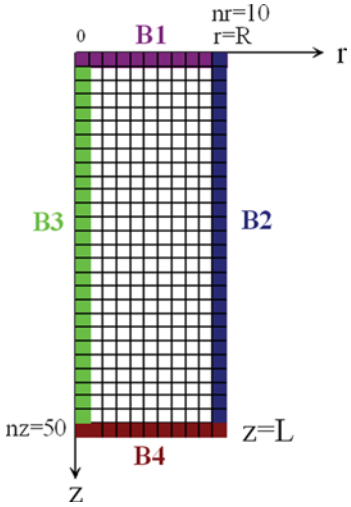

Fig. 4. Mesh of the 2D hydrocracking model on the z-r plane.

B1: At the inlet of the reactor (z=0)

$$u=\frac{m_f^0}{\pi R_r^2 \rho_f} \text{ and } v=0 \quad (20)$$

$$C_f=\rho_f,\ C_{D,N,G}=0 \text{ and } P=146 \text{ bar} \quad (21)$$

where R_r is the radius of the reactor, and m_f^0 is the mass flow rate of the feed.

B2: At the wall ($r=R_r$)

No slip condition: u=v=0 (22)

$$\frac{\partial C_j}{\partial r}=0 \text{ and } \frac{\partial P}{\partial r}=0 \quad (23)$$

B3: At the center (symmetry) line (r=0)

$$\frac{\partial u}{\partial r}=\frac{\partial v}{\partial r}=\frac{\partial C_j}{\partial r}=\frac{\partial P}{\partial r}=0 \quad (24)$$

B4: at the outlet (z=L)

$$\frac{\partial u}{\partial z}=\frac{\partial P}{\partial z}=0 \text{ and } v=0 \quad (25)$$

Boundary conditions expressed in Eq. (20) and Eq. (25) (B1 and B4) are valid due to using inert particles at the inlet and outlet of the catalytic bed. Hence, a uniform flow without radial disturbances is expectable. Finally, for each lump, the average concentration is defined according to the following equation at the outlet boundary (B4):

$$C_{j,av}=\frac{\int_{z=L} 2\pi r C_j(z,r)dr}{\int_{z=L} 2\pi r dr} \quad (26)$$

After solving the described equations, for estimating the kinetic parameters, the sum of squared error is minimized as follows:

$$SQE=\sum_{n=1}^{N_t}\sum_{j=F}^{G}\left(Y_{jn,ave}^{meas}-Y_{jn,ave}^{pred}\right)^2 \quad (27)$$

In Eq. (27), N_t, Y_{jn}^{meas} and $Y_{jn,ave}^{pred}$ are the number of test runs, the measured and the average predicted yields, respectively.

To develop the 2D model, Aspen Custom Modeler (ACM) programming environment is used. Fig. 4 shows the solution domain of the system mapped on the z-r plane. To discretize the domain and sub-domain equations, the "BFD2" (2nd order backward finite differences) method is applied. Then, Eq. (27) is minimized by the NL2SOL algorithm available in the ACM software.

To evaluate the estimated kinetic parameters, the average absolute deviation (AAD%) and the mean square error (MSE%) of the prediction are calculated using the following expressions:

$$AAD\%=\frac{\sum_{n=1}^{N_t}\sum_{j=F}^{G}\sqrt{\frac{\left(Y_{jn}^{meas}-Y_{jn,ave}^{pred}\right)^2}{\left(Y_{jn}^{meas}\right)^2}}}{N_t}\times 100 \quad (28)$$

$$MSE\%=\frac{\sum_{n=1}^{N_t}\sum_{j=F}^{G}\left(Y_{jn}^{meas}-Y_{jn,ave}^{pred}\right)^2}{N_t}\times 10^4 \quad (29)$$

RESULTS AND DISCUSSION

The model equations are coded in the ACM, and they are solved by using the kinetic parameters of 1D model [24] as initial values. Because all paths contribute in the reaction network (Fig. 2), the model is called a complete one. The values of radial and axial meshes (n_r and n_z) are selected equal to 10 and 50, respectively. After minimizing Eq. (27), kinetic parameters are re-estimated. Then, the 2D model is solved to predict yields of gas, naphtha, distillate and residue.

In Tables 5 and 6, the AAD% and MSE% of the 1D and 2D models are tabulated, respectively. One can find that both AAD% and MSE% of gas, naphtha and distillate are acceptably decreased, especially for the gas lump. The latter have a low accuracy when it is predicted by the 1D model. However, for the residue lump, the prediction of 1D complete model is more accurate than the 2D one. But, it is obvious that among hydrocracking products, yields of gas, distillate and naphtha are more important than the residue for evaluating the catalyst performance, and also economy of the process. Thus, the 2D model is more reliable to predict the yield of the hydrocracking products.

In Table 7, kinetic constants and order of reaction rates at the

Table 5. The comparison of AAD% between 1D and 2D models

Lump	1D (Complete)	1D (Reduced)	2D (Complete)	2D (Reduced)
Gas	21.04	20.7	14.13	14.10
Naphtha	4.92	5.34	3.77	3.76
Distillate	5.33	5.11	3.41	3.41
Residue	1.83	1.76	2.13	2.13
Ave.	8.28	8.23	5.86	5.85

Table 6. The comparison of MSE% between 1D and 2D models

Lump	1D (Complete)	1D (Reduced)	2D (Complete)	2D (Reduced)
Gas	0.171	0.152	0.095	0.095
Naphtha	0.213	0.236	0.197	0.196
Distillate	2.243	2.152	1.084	1.084
Residue	1.760	1.704	2.290	2.290
Ave.	1.096	1.061	0.917	0.916

Table 7. Kinetic parameters for the complete network of the 2D model

Frequency factor ($m^3 \cdot s^{-1} \cdot m^3\ cat^{-1}$)		Activation energy (kcal/mol)		Rate order	
k_{0FD}	29.88	E_{FD}	14.37	k_{FD}	1
k_{0FN}	26532.8	E_{FN}	24.53	k_{FN}	0.331
k_{0FG}	48	E_{FG}	18.18	k_{FG}	0.083
k_{0DN}	0.0059	E_{DN}	5.4	k_{DN}	0.21
k_{0DG}	0.052	E_{DG}	51.43	k_{DG}	0
k_{0NG}	<1E-10	E_{NG}	0	k_{NG}	0

average operating temperature (375 °C) are presented. For the 2D complete model, the rate order of converting distillate to gas (k_{DG}) is significantly lower than the highest value (k_{FD}). Thus, this reaction can be ignored. Moreover, it is concluded that in the studied operating temperature, the activation energy for hydrocracking of naphtha to gas is independent of temperature. The reason for this phenomenon is the higher activity of zeolite based catalysts for promoting hydrocracking reactions.

Additionally, as seen in Table 7, the apparent activation energies of VGO to distillate, naphtha and gas (k_{FD}, k_{FN} and k_{FG}) are 14.37 kcal/mol, 24.53 kcal/mol and 18.18 kcal/mol, respectively. The reported ones by Aboul-Ghiet [13] are about 13-17.5 kcal/mol, 22-24 kcal/mol and 18-19 kcal/mol, respectively. Therefore, the values reported in this work are reasonable. Additionally, the reported activation energy for the formation of naphtha from middle distillate at low temperatures (340 °C to 370 °C) is approximately 8.8 kcal/mol [32]. Therefore, the activation energy estimated in this research (i.e., 5.4 kcal/mol) is acceptable. It is supposed that the lower value is due to the higher activity of the zeolite based catalysts.

To reduce the number of model parameters, negligible values in Table 7 (k_{0DG}, k_{0NG}, E_{DG}, E_{NG}) are ignored during parameter estimation. Therefore, a reduced reaction network is generated (see Fig. 5). Now, eight remaining model parameters are re-estimated by using the measured data. The kinetic parameters of 2D reduced network are presented in Table 8.

Comparison between the simulated and measured yields confirms that the AAD% and MSE% of the 2D reduced network decrease to 5.85% and 0.916%, respectively, which are lower than the 2D complete network.

Furthermore, comparisons of predicted yields obtained by the 2D reduced model against the experimental ones are shown in Figs. 6 to 9. There is a close mapping between the measured and the predicted yields, and also yields predicted by 2D reduced model are in good agreement with the experimental observations. To have

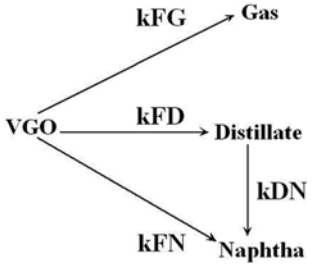

Fig. 5. The reduced four-lump kinetic network for the 2D bed model.

Table 8. Model parameters for the reduced network of 2D model

Kinetic parameters			
Frequency factor ($m^3 \cdot s^{-1} \cdot m^3$ cat^{-1})		Activation energy (kcal/mol)	
k_{0FD}	29.87	E_{FD}	14.37
k_{0FN}	26891.9	E_{FN}	24.55
k_{0FG}	49.233	E_{FG}	18.22
k_{0DN}	0.006	E_{DN}	5.4
k_{0DG}	-	E_{DG}	-
k_{0NG}	-	E_{NG}	-

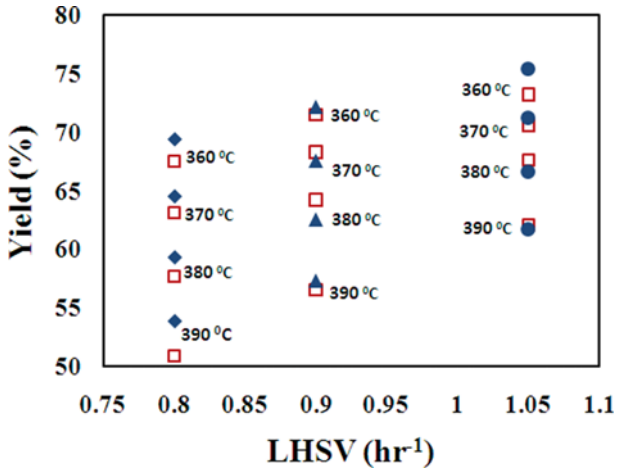

Fig. 6. Predicted (◆, ▲ & ●) and measured (□, △ & ○) yields of VGO.

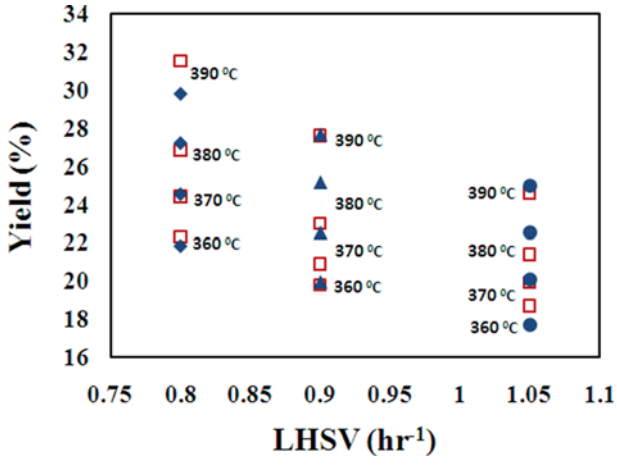

Fig. 7. Predicted (◆, ▲ & ●) and measured (□, △ & ○) yields of distillate.

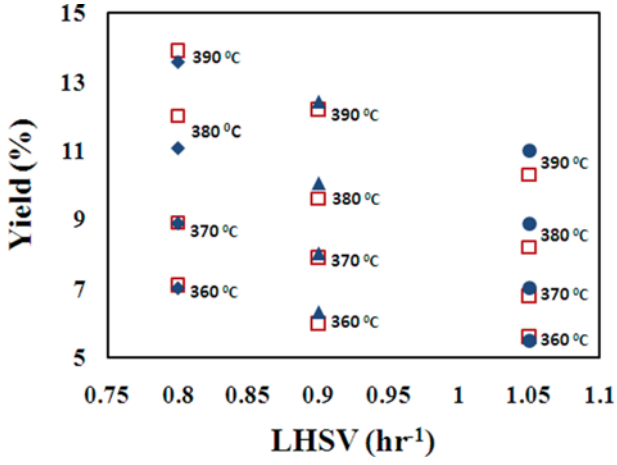

Fig.8. Predicted (◆, ▲ & ●) and measured (□, △ & ○) yields of naphtha.

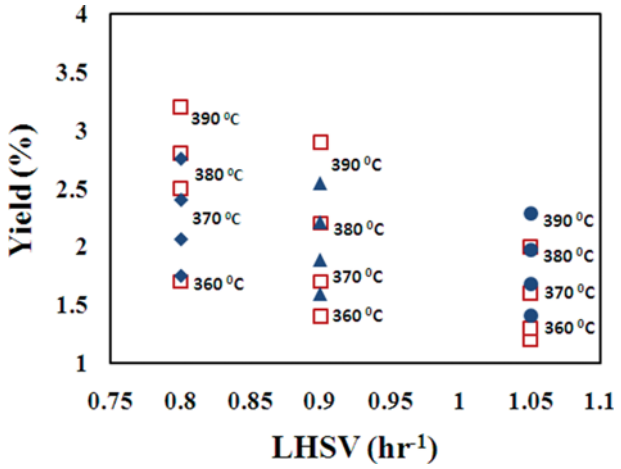

Fig. 9. Predicted (◆, ▲ & ●) and measured (□, △ & ○) yields of gas.

a better judgment, the AAD% and MSE% of the complete and reduced 1D models are shown in Tables 5 and 6, respectively. From these tables, it can be understood that for all lumps, 2D model is more efficient than the 1D one, except to the residue which can be predicted more accurately by the 1D model.

The contour plots in Figs. 10(a) and 10(b) reveal the radial velocity (V_r) distribution calculated by the CFD model at the lowest (LHSV=0.8 h^{-1} and T=370 °C), and the highest design temperatures (LHSV=0.8 h^{-1} and T=390 °C), respectively. In these figures, the right and left ends of the X-axis show the wall and center of the reactor, respectively. From the center of the reactor (r=0) to the area close to the center (r=2 mm), there is no significant radial liquid velocity. However, from r=2 mm to the adjacent of the wall (i.e., r=7.5 mm), the magnitude of radial velocity increases to reach a maximum. After that, it is gradually reduced to zero to reach the wall. Moreover, from the inlet of the reactor, the radial velocity grows gradually due to decreasing viscosity and density of the liquid flow. But, at the outlet of reactor, it vanishes because of uniform flow created by using the SiC particles.

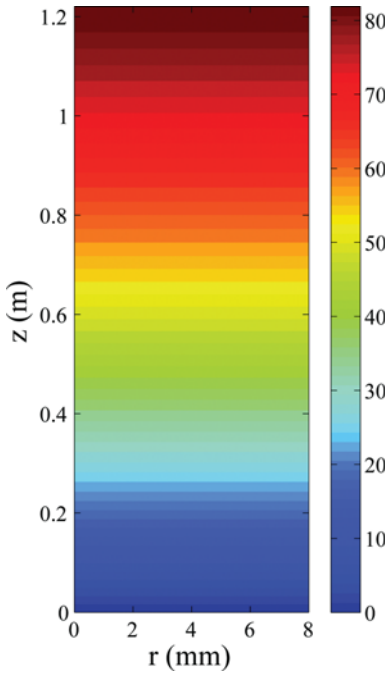

Fig. 11. Distribution of the pressure drop through the catalytic bed.

The comparison between Fig. 10(a) and Fig. 10(b) confirms that the magnitude of radial liquid velocity is more significant at higher temperatures. However, its order of magnitude is less than (−8). It is obvious that lower density and viscosity of the stream at higher temperatures increase the radial liquid velocities through the catalytic bed.

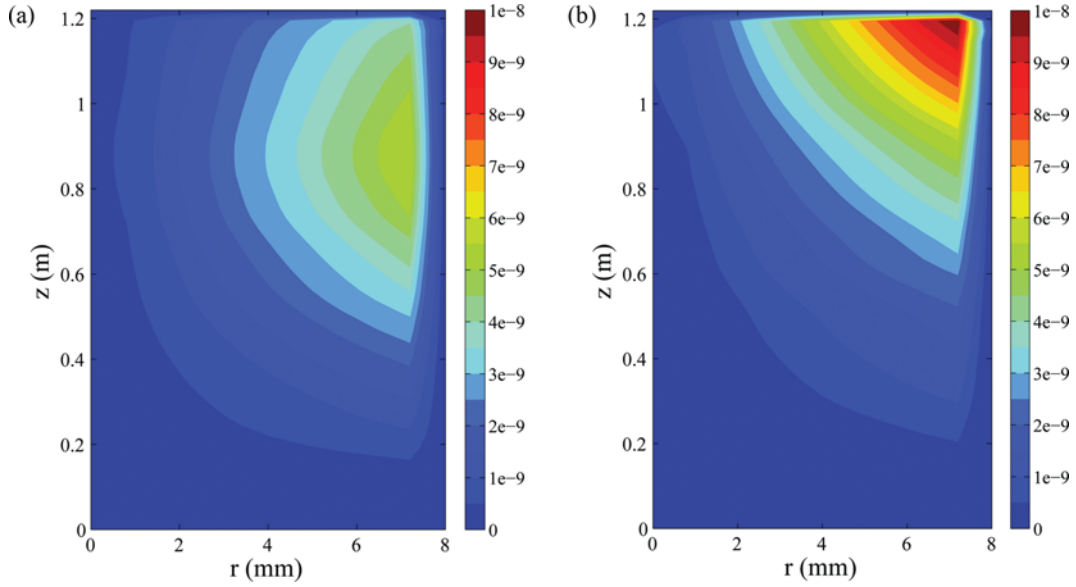

Fig. 10. (a) Distribution of the radial liquid velocity (m/h) in the catalytic bed (LHSV=0.8 h^{-1}, T=370 °C). (b) Distribution of the radial liquid velocity (m/h) in the catalytic bed (LHSV=0.8 h^{-1}, T=390 °C).

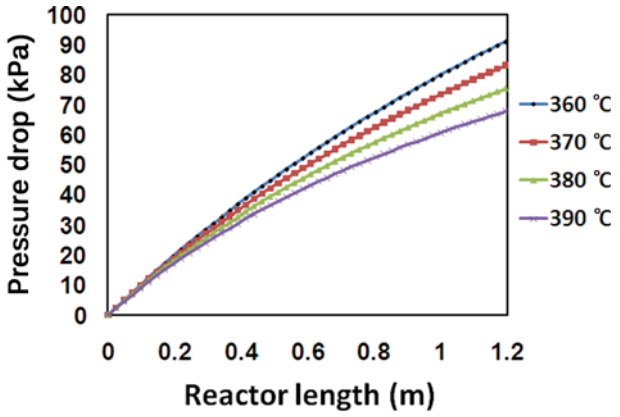

Fig. 12. Effect of temperature on pressure drop at LHSV=0.8 h^{-1}.

In Fig. 11, contour plots of pressure drop through the catalytic bed at LHSV=0.8 h^{-1} and T=370 °C are depicted. At a specific axial point, there is no considerable pressure gradient in the radial direction. Therefore, the pressure drop along the r-direction is not significant.

In Fig. 12, the pressure drop of the catalytic bed through the z-direction at different temperatures and the constant LHSV of 0.8 h^{-1} (design value) is presented. In contrast with the r-direction, the pressure drop along the z-direction is significant which is between 60 kPa and 100 kPa (49.18 kPa<Δp/L<81.96 kPa). As seen, by increasing the temperature, the pressure drop decreases due to the lower viscous forces at the higher temperatures. Thus, the higher temperatures are not only more preferable for the higher conversion, but also more favorable due to the lower pressure drop and the mechanical energy loss in TBRs. The experimental measurement for a concurrent down flow TBR loaded with 1.4 mm glass beads and reactor diameter of 2.3 cm without reaction (polypropylene carbonate and nitrogen and helium) shows a Δp/L from 60 kPa to 140 kPa [33], confirming the acceptable value of the pressure drop calculated in the current research. This parameter is very significant for designing, scaling up and evaluating the cost of the process.

Fig. 13 illustrates the variations of liquid holdup by increasing the temperature. At the beginning of the bed (0<z<0.1 m), the holdup

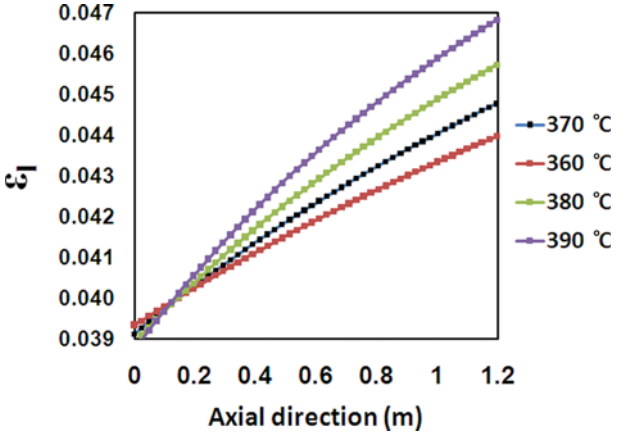

Fig. 13. Effect of temperature on liquid hold up at LHSV=0.8 h^{-1}.

is lower because of the lower density of gas at higher temperatures. But, after a short distance, the hydrocracking reactions shift the density of the liquid to the lower values. Consequently, the holdup of the liquid increases rapidly. As seen, from z=0.15 m, the holdup of liquid is suddenly shifted to the higher values. From these results, it is revealed that elevating the temperature for hydrocracking process in a TBR not only does promote corresponding reactions, but also increases the volume of the liquid. The latter can significantly enhance the efficiency of the process.

CONCLUSION

A VGO hydrocracking reactor was modeled using a 2D model in which continuity and momentum balance equations were solved simultaneously. Then, the predictability of the proposed model was validated using the reported experimental data in the literature.

The numerical simulations showed that the yields of a pilot scale VGO hydrocracker could be predicted with the AAD% and MSE% of 5.85% and 0.916%, respectively. In comparison to the 1D model, the predicted yields of the gas, naphtha and distillate were appreciably improved.

The results confirmed that the values of activation energies and pressure drop along the bed were in compatible with the reported ones in the literature. Moreover, higher temperatures were more favorable in the hydrocracking process because of higher conversion, the lower pressure drop and the higher efficiency of the catalytic bed. These factors can significantly influence economics of the process. But, the temperature of the catalytic bed should be set meticulously to inhibit excess coke formation on the catalyst surface.

NOMENCLATURE

Notations

C : mass concentration $(kg/m)^3$
d_p : diameter of the catalyst (1/16″)
D : distillate
D_{jf} : molecular diffusion of lump j in VGO feed [cm^2/s]
D_r : internal diameter of the reactor [1.6 cm]
E : apparent activation energy [kcal/mol]
F : drag force
g_r : gravitational force in the r direction [0 m/s^2]
g_z : gravitational force in the z direction [9.806 m/s^2]
G : gas
k : reaction rate constant [$m^3 \cdot s^{-1} \cdot m^3\ cat^{-1}$]
k_0 : frequency factor [$m^3 \cdot s^{-1} \cdot m^3\ cat^{-1}$]
L : length of the catalytic bed [1.22 m]
m^0 : mass flow rate [kg/h]
n_r : number of meshes in the radial direction [-]
n_z : number of meshes in the axial direction [-]
Mw : molecular weight [-]
N : naphtha [-]
N_t : number of experiments [-]
P : pressure [kPa]
r : radius in cylindrical coordinate [m]
R_j : reaction rate of lump j [$kg \cdot s^{-1} \cdot m^3\ cat^{-1}$]
S_l : volume fraction of liquid in the void of catalytic bed [-]

T : temperature [K]
u : superficial liquid velocity at axial direction [m/s]
U : superficial liquid velocity [m/s]
v : superficial liquid velocity at radial direction [m/s]
V : molar volume [kmol/m^3]
Y : yield of products [-]
z : length in the cylindrical coordinate [m]

Greek Letters

α : velocity parameter [-]
ε : bed void fraction [-]
ε_l : liquid hold up of catalytic bed [-]
η : effectiveness factor [-]
μ : viscosity [Pa·s]
$\dot{v}_m$: volume flow rate of the liquid [m^3/s]
$\dot{v}_{H_2}$: volume flow rate of the gas [m^3/s]
ρ : density [kg/m^3]

Subscripts

c : coefficient in the velocity correlation [-]
F_j : feed to lighter lumps
j : distillate, naphtha and gas lumps
j′ : naphtha and gas lumps

REFERENCES

1. C. S. Laxminarasimhan and P. A. Ramachandran, *AIChE J.*, **42**(9), 2645 (1996).
2. L. Joonwon, H. Sunhwan, L. Sang-bong and I. K. Song, *Korean J. Chem. Eng.*, **27**(6), 1755 (2010).
3. S. Yoon, W. C. Choi, Y. K. Park, H. Y. Kim and C. W. Lee, *Korean J. Chem. Eng.*, **27**(1), 62 (2010).
4. P. Balasubramanian and S. Pushpavanam, *Fuel*, **87**, 1660 (2008).
5. S. Zahedi Abghari, J. Towfighi Darian, R. Karimzadeh and M. R. Omidkhah, *Korean J. Chem. Eng.*, **25**(4), 681 (2008).
6. S. Zahedi Abghari, S. Shokri, B. Baloochi, M. Ahmadi Marvast, S. Ghanizadeh and B. Afshin, *Korean J. Chem. Eng.*, **28**(1), 93 (2011).
7. S. Zahedi, R. Hayati, S. Sadighi and M. Bayat, *Korean J. Chem. Eng.*, **32**(4), 629 (2015).
8. G. Bozzano, M. Dente and F. Carlucci, *Comput. Chem. Eng.*, **29**, 1439 (2005).
9. I. Elizalde, M. A. Rodrıguez and J. Ancheyta, *Appl. Catal. A-Gen.*, **365**, 237 (2009).
10. I. Elizalde and J. Ancheyta, *Fuel*, **90**, 3542 (2011).
11. M. A. Callejas and T. Martinez, *Ind. Eng. Chem. Res.*, **38**, 98 (1999).
12. K. Aoyagi, W. C. McCaffrey and M. R. Gray, *Pet. Sci. Technol.*, **21**, 997 (2003).
13. K. Aboul-Gheit, *Erdol Kohle Erdgas*, **105**, 1278 (1989).
14. G. Valavarasu, M. Bhaskar and B. Sairam, *Pet. Sci. Technol.*, **23**, 1323 (2005).
15. R. M. Almeida and R. Guirardello, *Catal. Today*, **109**, 104 (2005).
16. S. Sadighi, A. Arshad and S. R. Mohaddecy, *Int. J. Chem. React. Eng.*, **8**(A1), 1 (2010).
17. S. Sadighi and A. Ahmad, *Can. J. Chem. Eng.*, **97**, 1077 (2013).
18. H. A. Jakobsen, H. Lindborg and V. Handeland, *Comput. Chem. Eng.*, **26**, 333 (2007).
19. P. R. Gunjal and V. V. Ranade, *Chem. Eng. Sci.*, **62**, 5512 (2007).
20. J. G. Lopes Rodrigo and R. M. Quinta-Ferreira, *Chem. Eng. Sci.*, **64**, 1806 (2009).
21. F. Augier, A. Koudil, A. Royon-Lebeaud, L. Muszynski and Q. Yanouri, *Chem. Eng. Sci.*, **65**, 255 (2010).
22. J. G. Lopes Rodrigo, S. L. Sousa Vera and R. M. Quinta-Ferreira, *Chem. Eng. Sci.*, **66**, 3280 (2011).
23. M. R. Bandari, Y. Behjat and S. Shahhosseini, *Int. J. Chem. React. Eng.*, **10**(1), 1 (2012).
24. S. Sadighi, A. Ahmad and M. Shirvani, *Int. J. Chem. React. Eng.*, **9**(A4), 1 (2011).
25. S. Sadighi, A. Arshad and M. Rashidzadeh, *Korean J. Chem. Eng.*, **27**(4), 1099 (2010).
26. R. G. Tailleur, *Comput. Chem. Eng.*, **29**, 2404 (2005).
27. G. Mary, J. Chaouki and F. Luck, *Int. J. Chem. React. Eng.*, **7**(A1), 1 (2009).
28. S. Liu and J. H. Masliyah, *J. Non-Newton. Fluid.*, **86**, 229 (1999).
29. P. L. Mills and M. P. Dudukovic, *Ind. Eng. Chem. Fund.*, **18**, 2 (1979).
30. F. S. Mederos, J. Ancheyta and J. Chen, *Appl. Catal. A: Gen.*, **355**, 1 (2009).
31. G. Latini, R. C. Grifoni and G. Passerini, UK, WIT Press (2006).
32. C. Botchwey, A. K. Dalai and J. Adjaye, *Can. J. Chem. Eng.*, **82**, 478 (2004).
33. M. H. Al-Dahhan, F. Larachi, M. P. Dudukovic and A. Laurent, *Ind. Eng. Chem. Res.*, **36**, 3292 (1997).